Synthesis, structure and physical properties of ternary Ce-based compound Ce_3VAs_5

B S Min(闵保森)[1,2], L C Fu(傅立承)[1,3], X M Chen(陈晓铭)[1,4], L C Shi(史鲁川)[1,2], H Y Zheng(郑皓宇)[1,4], J Zhang(张俊)[1], J Song(宋静)[1], Z Deng(邓正)[1], J F Zhao(赵建发)[1], L Duan(段磊)[4], C J Xiao(肖长江)[4], J L Zhu(朱金龙)[3,5], X C Wang(望贤成)[1,2,†], and C Q Jin(靳常青)[1,2,‡]

[1] *Beijing National Laboratory for Condensed Matter Physics, Institute of Physics, Chinese Academy of Sciences, Beijing* 100190, *China*
[2] *School of Physics, University of Chinese Academy of Sciences, Beijing* 100190, *China*
[3] *Department of Physics, Southern University of Science and Technology, Shenzhen* 518055, *China*
[4] *School of Materials Science and Engineering, Henan University of Technology, Zhengzhou* 450007, *China*
[5] *Quantum Science Center of Guangdong–Hong Kong–Macao Greater Bay Area (Guangdong), Shenzhen* 518045, *China*

(Received 12 September 2025; revised manuscript received 5 November 2025; accepted manuscript online November 2025)

A new Ce-based compound Ce_3VAs_5 has been synthesized at high-pressure and high-temperature conditions. The physical properties were investigated through the crystal structure, magnetism, electrical transport, and specific heat measurements. The compound crystallizes in a hexagonal Hf_5Sn_3Cu-anti-type structure with the space group of $P6_3/mcm$, which consists of face-sharing octahedral VAs_6 chains and zig-zag like Ce-chains along the c axis. It undergoes a ferromagnetic-like ordering at $T_N = 14$ K due to the Ce-lattice, and exhibits heavy fermion behavior with a Sommerfeld coefficient of $\gamma \sim 128$ mJ/(Ce-mol·K^2). The Kondo temperature T_K is determined to be ~ 19 K. The deviation of paramagnetic susceptibility from Curie–Weiss law is related to the crystal electric field (CEF) effects, and the abnormal drop in the resistivity is attributed to the synergistic interaction between CEF effect and Kondo scattering. Due to its quasi one-dimensional structure, Ce_3VAs_5 provides a good opportunity to study the anisotropy relative to Kondo effect in the future.

Keywords: heavy fermion, Kondo effect, Ce-based compound, antiferromagnetism

PACS: 71.27.+a, 72.15.Qm, 76.50.+g

DOI: 10.1088/1674-1056/ae1ded **CSTR:** 32038.14.CPB.ae1ded

1. Introduction

Heavy fermion system has attracted much research interest due to its rich physical phenomena,[1,10] such as heavy fermion superconductivity (SC),[1,4] In the system, there exist two competing couplings of Kondo interaction and Ruderman–Kittel–Kasuya–Yosida (RKKY) interaction, both of which are related with the coupling between the conducting electrons and local f-electrons (c–f coupling). RKKY interaction tends to form long-range magnetic order, while Kondo interactions destroy the magnetic order via the local moment screening. The physics dependent on c–f coupling strength J and the competition between Kondo interaction and RKKY interaction can be described by the Doniach's phase diagram.[11] When J is weak, the RKKY interaction dominates the system and leads to the formation of magnetism. While with increasing J, the Kondo interaction would become important and the magnetic ordering is gradually suppressed. Heavy fermion SC usually appears near a quantum critical point,[2,4] where the magnetic transition temperature is just suppressed to zero. Further increasing the J, the system will enter into a Fermi liquid state with a very large Sommerfeld coefficient γ. Besides the Doniach's picture, a two-fluid model also has been used to describe the physical picture in the heavy Fermion system,[12,15] where the Kondo coherent temperature T^* is a very important physical parameter. Above T^*, the local f electrons at each lattice site act as single-ion magnetic impurities, and the Kondo scattering is incoherent and usually increases the resistivity. While below T^*, the f band is hybridized with the conducting band, which generates a flat band with itinerant f characters via renormalization to form itinerant heavy fermions. Thus, in the picture of two-fluid model, local and itinerant f characters coexist and respond to the magnetism (spin liquid) and heavy fermions (Kondo liquid), respectively.

The compounds with Hf_5Sn_3Cu-antitype structure have been extensively studied, and much attention is focused on the physics related to the quasi-1D spin chains because of their quasi one-dimensional (1D) structure character.[16,29] For example, $Ba_6Cr_2S_{10}$ consists of face-sharing octahedral CrS_6 chains separated with a large distance more than 9 Å, thus demonstrating typical quasi-1D spin chain character and exhibiting strong magnetic fluctuation.[16] Nevertheless, for the Ce_3TiX_5 (X = As, Sb and Bi) system, the magnetism arises from the Ce-lattice, and the physics related to the Kondo effect have been studied.[30,36] Their Sommerfeld coefficient γ

†Corresponding author. E-mail: wangxiancheng@iphy.ac.cn
‡Corresponding author. E-mail: Jin@iphy.ac.cn

values are about 200 mJ/(Ce-mol·K^2), demonstrating heavy Fermion behavior. The magnetic transition temperature T_N was reported to increase from $\sim$ 5 K to $\sim$ 13 K when the anion X varies from Bi to As, which suggests the RKKY interaction is predominant in the system. In addition, in Ce_3TiX_5, the interaction between the crystal electric field (CEF) and the Kondo effect has been reflected by the broad maximum or quick drop in the resistivity curve.[30,32]

In this work, we successfully synthesized the new compound of Ce_3VAs_5 by substituting V for Ti in Ce_3TiAs_5. This material exhibits a ferromagnetic-like order at 14 K, a Sommerfeld coefficient of γ of $\sim$ 128 mJ/(Ce-mol·K^2) and a Kondo temperature of $\sim$ 19 K. Furthermore, an anomalous drop in the resistivity suggests a cooperative effect between CEF and Kondo scattering.

2. Experiments

Polycrystalline samples of Ce_3VAs_5 were synthesized at high-pressure and high-temperature conditions. The precursor CeAs was prepared by heating a mixture of Ce flakes (Alfa, 99.9%) and As powder (Alfa, 99.99%) in a vacuum quartz tube at 700 °C for 10 hours. Subsequently, the obtained CeAs powder was mixed with V powder (Alfa, 99.99%) and As powder in a molar ratio of 3:1:2. The mixture was ground and pressed into a pellet, and then was put into an hBN crucible and sintered at 1400 °C for 30 min at 5 GPa by using a cubic anvil high-pressure apparatus. Finally, we obtained the black polycrystalline Ce_3VAs_5 samples.

The powder x-ray diffraction (XRD) experiments were carried out on a Rigaku Ultima diffractometer. The data were collected at a scanning rate of 5°/min with a scanning step length of 0.005°. The Rietveld refinement on the diffraction spectra was conducted with the GSAS and EXPGUI packages.[37] DC magnetization measurements were performed using a Quantum Design magnetic property measurement system (MPMS). AC magnetic susceptibility was measured with an applied field of $H_{AC} = 1$ Oe. Electrical resistivity was measured using a standard four-probe technique. The AC magnetic susceptibility, resistivity and heat capacity measurements were carried out on a Quantum Design physical property measurement system (PPMS).

3. Results and discussion

The x-ray diffraction pattern and the corresponding Rietveld refinement for the Ce_3VAs_5 sample are presented in Fig. 1(a). All the peaks can be indexed to a hexagonal structure with $a = b = 8.851$ Å and $c = 5.808$ Å, and the lattice constants of which are slightly smaller than that of Ce_3TiAs_5.[32] By using the crystal structure of Ce_3TiSb_5 with the space group of $P6_3/mcm$ as the initial structural model,[38] the Rietveld refinement was performed and smoothly converged to $R_p = 4.7\%$, $R_{wp} = 6.3\%$. Table 1 presents the summarized crystallographic data, and figure 1(b) displays a schematic crystal structure of Ce_3VAs_5 viewed along the c-axis. It consists of face-sharing octahedral VAs_6 chains, As-chains and zig-zag like Ce-chains along the c axis. The VAs_6 chains are separated by $a = 8.851$ Å, demonstrating quasi-1D spin chain structural character. For the zig-zag like Ce-chains, the intrachain Ce–Ce distance is about 3.598 Å, which is slightly smaller than the interchain distance given by $a/2$ $\sim$ 4.425 Å. This means the Ce-lattice in Ce_3VAs_5 is more three-dimensional.

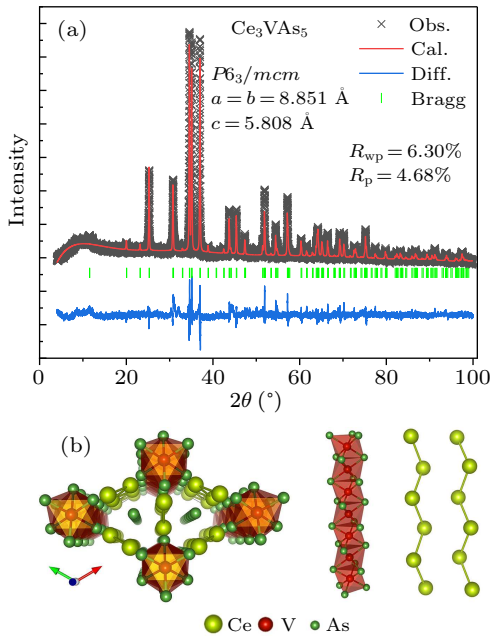

Fig. 1. (a) XRD pattern and the corresponding Rietveld refinement for the polycrystalline Ce_3VAs_5 sample. (b) Crystal structure viewed along the c-axis, highlighting the quasi-1D structural character.

Table 1. Crystallographic data for Ce_3VAs_5.

Ce_3VAs_5 hexagonal ($P6_3/mcm$) $a = b = 8.851(7)$ Å, $c = 5.808(6)$ Å, $V = 394.1(4)$ Å^3 $R_p = 4.7\%$, $R_{wp} = 6.3\%$						
Atom	Wyck.	x	y	z	Occ.	Uiso
Ce	6g	0.6200	0	0.25	1	0.03(5)
V	2b	0	0	0	1	0.01(9)
As(1)	6g	0.2474	0	0.25	1	0.02(0)
As(2)	4d	0.3333	0.6667	0	1	0.04(6)
d_{intra} (Ce–Ce) = 3.598(3) Å; d_{inter} (Ce–Ce) = 4.425(8) Å; d_{intra} (V–V) = 2.904(3) Å; d_{inter} (V–V) = 8.851(7) Å; d_{intra} (As–As) = 2.904(3) Å						

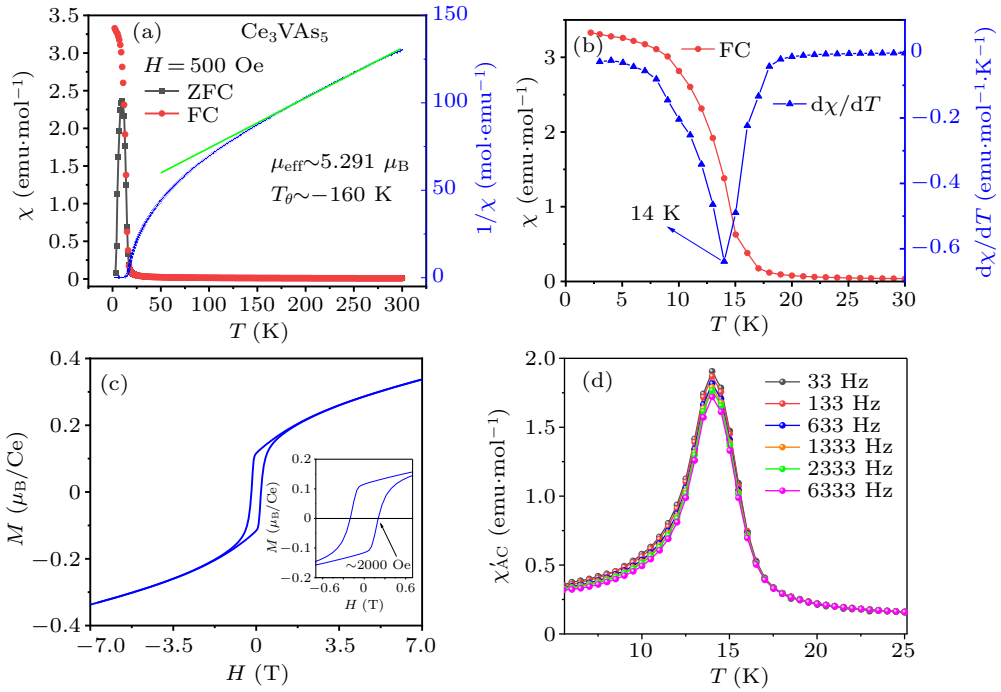

Fig. 2. (a) Temperature dependence of magnetic susceptibility for Ce_3VAs_5 measured under an applied field of 500 Oe. The blue curve represents the inverse susceptibility $1/\chi(T)$, with the green line showing the linear Curie–Weiss fit. (b) An enlarged view of the $\chi(T)$ curve and its temperature derivative $\mathrm{d}\chi/\mathrm{d}T$. (c) Magnetization as a function of magnetic field measured at 2 K. The inset shows an enlarged view to reveal the coercive field. (d) AC magnetic susceptibility measured at different frequencies.

Figure 2(a) displays the temperature dependence of the magnetic susceptibility for the Ce_3VAs_5 sample, which was measured in both zero-field cooling (ZFC) and field cooling (FC) modes with the applied magnetic field $H = 500$ Oe. Below 25 K, the susceptibility increases sharply with lowering temperature, exhibiting ferromagnetic-like ordering behavior. A bifurcation between the ZFC and FC susceptibility curves is observed below ~ 11 K. The ZFC susceptibility exhibits a peak, followed by a sharp decrease upon further cooling. To determine the transition temperature T_N, we plot the $\mathrm{d}\chi/\mathrm{d}T$ versus temperature curve as shown in Fig. 2(b), from which the transition temperature can be identified to be ~ 14 K by the sharp peak. The T_N value is close to that observed in the Ce_3TiAs_5 (~ 13 K).[32] The compound La_3VAs_5 was also synthesized; however, the obtained sample contained impurities. No long-range magnetic order was observed in this material down to 2 K. Therefore, it is speculated that the aforementioned magnetic transition at 14 K in Ce_3VAs_5 should originate from the Ce-lattice. For the V-lattice, the absence of long-range magnetic order might be related to its 1D spin chain feature, which usually leads to strong magnetic fluctuation.

The $1/\chi(T)$ curve is also presented in Fig. 2(a). By using the Curie–Weiss (CW) formula $1/\chi = (T - \theta)/C$ to make a fit for the high-temperature paramagnetic data as shown with the green line, we can get the Weiss temperature $\theta = -160$ K and the effective magnetic moment $\mu_{eff} = 5.291(5)\ \mu_B$. The negative θ value indicates that antiferromagnetic (AFM) coupling between Ce-ions dominates the magnetic coupling in Ce_3VAs_5. For Ce_3TiX_5 (X = As, Sb, Bi) compounds, the experimentally determined μ_{eff} values agree with those expected for free Ce^{3+} ions.[30,32] Therefore, it is considered that the oxidation state of Ce ions in Ce_3VAs_5 should be +3 as well. Theoretically, for Ce_3VAs_5 the effective magnetic moment can be calculated with the formula of $\mu_{eff} = \sqrt{3g_{Ce}^2 J(J+1) + g_V^2 S(S+1)}\mu_B$, where $g_{Ce} = 6/7$ and $J = 5/2$ are the Landau g-factor and total angular momentum of the Ce^{3+} ion, respectively, and $g_V = 2$ and S denote the g-factor and spin momentum of V ions. Consequently, based on the experimentally obtained μ_{eff} value, the contribution to the effective moment from V ions can be estimated to be $\sim 2.952\ \mu_B$, corresponding to a local electron number $n \sim 2.1$. This implies that the oxidation state of V ions in Ce_3VAs_5 compound should be less than +3. Below ~ 150 K, the $1/\chi$ curve gradually deviates from the CW law, which should primarily arise from the reduction of local moment induced by CEF. This deviation of the magnetic susceptibility from the Curie–Weiss law due to CEF effect is usually observed below 300 K[30,32,39,40] in Ce-based compounds because the f orbital is an inner one and the CEF splitting energy is comparable with the energy scale of room temperature.

Figure 2(c) shows the magnetic field dependence of magnetization for the Ce_3VAs_5 sample measured at 2 K. There is a small hysteresis loop with the coercivity field about 2000 Oe. When the applied magnetic field exceeds 3 T, the magnetization almost increases linearly with increasing H and does not show signs of saturation within the highest experimental H. The magnetization at 2 K and 6.5 T is about 0.35 μ_B/Ce. Unlike the Ce_3TiX_5 (X = As, Sb and Bi),[30,32,35] no field induced

metamagnetic transition has been observed in Ce_3VAs_5.

The Ce_3TiX_5 compounds exhibit diverse and complex magnetic structures. Specifically, Ce_3TiBi_5 features a cycloid magnetic order,[36] whereas Ce_3TiSb_5 hosts two coexisting magnetic phases.[34] In the case of Ce_3TiAs_5, although it shows a ferromagnetic-like ordering behavior, its negative Weiss temperature indicates dominant AFM interactions. This AFM nature is further supported by a field-induced metamagnetic transition at a critical field $H_c \approx 0.7$ T.[32] Here, Ce_3VAs_5 displays similar magnetic properties to Ce_3TiAs_5, except for the absence of a metamagnetic transition. The linear field dependence of magnetization above 3 T, together with the low magnetization observed at 6.5 T (partially due to the Kondo screening), also point to dominant AFM coupling in Ce_3VAs_5. Furthermore, we have carried out the AC magnetic susceptibility measurements, as seen in Fig. 2(d). There is a peak centered at 14 K, same with the magnetic transition T_N, and the peak is independent on the frequencies. It is convincing that the magnetic transition is naturally an antiferromagnetic one. The coexistence of ferromagnetic-like behavior and dominant AFM coupling hints at a canted antiferromagnetic state, and the magnetic structure warrants further investigation.

Figure 3 displays the temperature dependence of the resistivity for Ce_3VAs_5 together with that of Ce_3TiAs_5 for comparison. Both compounds exhibit resistivity of comparable magnitude. In contrast to the normal metallic behavior observed in Ce_3TiAs_5, the resistivity of Ce_3VAs_5 shows almost linear temperature dependence at high temperatures as indicated by the green line, which is likely due to the stronger Kondo scattering in Ce_3VAs_5. The resistivity starts to deviate from the straight line at $\sim$ 130 K and decreases faster and faster with lowered temperature. The inset of Fig. 3 illustrates the temperature derivative of resistivity $d\rho/dT$ near T_N. The $d\rho/dT$ curve obviously shows a dramatic change at 14 K, further indicating the occurrence of the magnetic transition. The linear-deviation temperature in resistivity is close to that where the susceptibility data deviates from CW behavior, suggesting the resistivity drop is also related to the CEF effect. In fact, this abnormal decrease of resistivity is usually observed in other Ce-based heavy fermion compounds[30,32,41] and can be explained by the synergistic effects of the CEF effect and Kondo scattering. The CEF effect induces a degenerate lifting of the Ce-4f energy levels with the excitation energy Δ/K_B being typically less than 300 K. As temperature decreases across the temperature of Δ/K_B, Ce-4f electrons would gradually transfer from the upper excited energy level to the lower one. Since the lower excited energy level is further away from the Fermi energy level, the c–f coupling between the f electrons on the lower energy level and conduction electrons would be weaker, i.e., the Kondo scattering is smaller. Consequently, the resistivity would undergo an abnormal drop when temperature decreases across Δ/K_B. Therefore, from the abnormal temperature of 130–150 K in magnetic susceptibility and resistivity data, one of the CEF split excited energy levels can be coarsely estimated to be 11.2–12.9 meV.

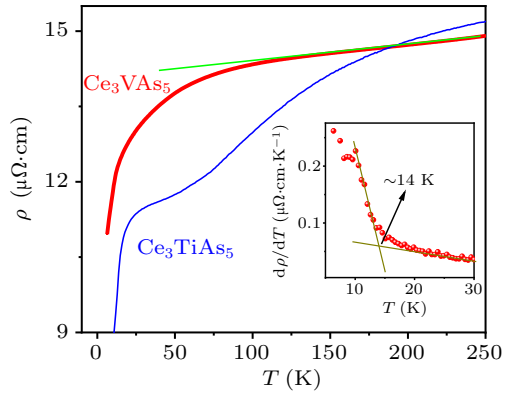

Fig. 3. Temperature dependence of resistivity for Ce_3VAs_5 together with that of Ce_3TiAs_5. The green straight line is drawn by eyes to show the linear temperature dependence of resistivity. The inset shows $d\rho/dT$ versus temperature near T_N.

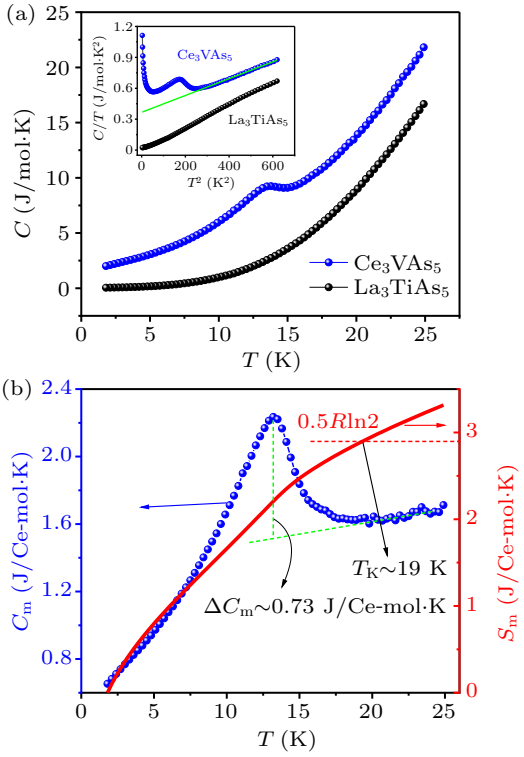

Fig. 4. (a) Temperature dependence of heat capacity $C(T)$ for Ce_3VAs_5. The inset shows C/T versus T^2, where the green line is the linear fitting just above T_N. (b) Temperature dependence of magnetic heat capacity and the entropy change.

Figure 4(a) presents the temperature dependence of heat capacity $C(T)$ for Ce_3VAs_5 with the data of La_3TiAs_5 for comparison. The magnetic transition can be further evidenced by the heat capacity jump at $\sim$ 14 K. The inset illustrates the C/T versus T^2 curve. Above T_N, a fitting was carried out by using the equation $C/T = \gamma + \beta T^2$, where γ and β are the coefficients of the electron and lattice contributions to the heat capacity, respectively. The fitting yields the $\gamma \sim 128$ mJ/(Ce-

mol·K^2) and $\beta \sim 0.000768$ J/(mol·K^4). The Debye temperature Θ_D of Ce_3VAs_5 is estimated to be ~ 283 K by using the formula $\Theta_D = (12\pi^4 Rn/5\beta)^{1/3}$, where $n = 9$ represents the number of atoms in the unit cell. The Sommerfeld coefficient γ, though smaller than the value (~ 215 mJ/(Ce-mol·K^2)) in the Ce_3TiAs_5 system,[32] nevertheless demonstrates the heavy fermion nature of Ce_3VAs_5. At low temperatures, C/T rises rapidly with lowering temperature, reaching ~ 390 mJ/(mol·K^2) at 2 K. Such an upturn of C/T at low temperatures has also been observed in Ce_3TiAs_5.[32] The anomalous upturn is commonly attributed to the Schottky anomaly. Alternatively, it might originate from the development of Kondo screening, which would lead to an enhancement of the Sommerfeld coefficient γ.

By subtracting the heat capacity of La_3TiAs_5 as the lattice contribution, we can coarsely get the magnetic heat capacity C_m. Figure 4(b) displays the temperature dependence of C_m, from which we can see a heat capacity jump of approximately 0.73 J/(Ce-mol·K) due to the magnetic transition, which is smaller than that in Ce_3TiAs_5 (1.2 J/(Ce-mol·K))[32] and in Ce_3TiSb_5 (3.9 J/(Ce-mol·K)).[30] By integrating C_m/T from 2 K to 25 K, the change of magnetic entropy S_m can be estimated to be ~ 3.3 J/(Ce-mol·K), which is much less than that of $R\ln(2S+1)$, where R denotes the gas constant and $S = 1/2$ is the effective spin for a doublet ground state. Such a small S_m change is related to its small heat capacity jump at T_N, and implies that part of the local Ce-f moments have been screened. The Kondo temperature T_K can be determined to be ~ 19 K by the temperature where the change of S_m reaches $0.5R\ln 2$, which is slightly higher than T_N.

Table 2 summarizes the some parameters in the Ce_3TiX_5 and Ce_3VAs_5 systems. The unit cell volume decreases in the order of X = Bi, Sb, As, with Ce_3VAs_5 exhibiting the smallest one. This reduction in volume can be viewed as a form of chemical pressure. All four compounds exhibit negative Weiss temperatures, indicating the predominance of antiferromagnetic coupling. The effective magnetic moments μ_{eff} are consistent with those expected for Ce^{3+} ions with $J = 5/2$, except in the case of Ce_3VAs_5, where an additional contribution from localized V spins is present. The chemical pressure dependence of the Néel temperature T_N and the Kondo temperature T_K are also shown in Fig. 5. Following the Doniach diagram, the light blue and orange shaded areas schematically represent the AFM and Fermi liquid regimes, respectively. Both the T_N and the T_K increase with chemical pressure, suggesting that although the Kondo screening effect is enhanced, the RKKY interaction remains dominant and governs the magnetic ground state. In addition, the heat capacity jump ΔC at T_N decreases under chemical pressure, reflecting the enhanced Kondo screening. The Sommerfeld coefficient γ is generally inversely proportional to the width of the Kondo resonance peak. Since this width is proportional to $k_B T_K$, γ is consequently negatively correlated with T_K. The T_K and γ values in the system seem to follow the negatively correlation except for Ce_3TiAs_5.

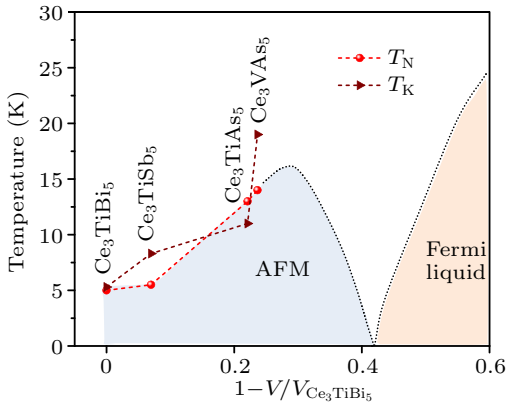

Fig. 5. The chemical pressure dependence of the Néel temperature T_N and the Kondo temperature T_K. Following the Doniach picture, the light blue and orange shaded areas schematically represent the AFM and Fermi liquid regimes, respectively.

Furthermore, similar to the Ce_3TiX_5, Ce_3VAs_5 is expected to host anisotropic Kondo effect due to its quasi-1D structural feature. Under high pressure, Ce_3TiBi_5 has been evidenced to exhibit anisotropic Kondo effect. For the resistivity along the c axis, the Kondo scattering dominates the transport behavior; while it has minor contribution to the resistivity in the direction perpendicular to the c axis.[33,42] In fact, the calculation is also carried out, further identifying the origin of the anisotropic Kondo effect as the strong anisotropic hybridization between the f and conduction bands.[42] Moreover, in the quasi-1D structures of Ce_3TiX_5 and Ce_3VAs_5, such an anisotropic hybridization would suppress electronic mass renormalization relative to 3D systems, consequently yielding a reduced Sommerfeld coefficient γ. A promising direction for future work is to explore the anisotropic Kondo effect in Ce_3VAs_5.

Table 2. Summary of the key parameters of the cell volume V, Néel temperature T_N, Weiss temperature θ, effective moment μ_{eff}, Kondo temperature T_K, Somerfield coefficient γ and heat capacity jump ΔC at T_N in the Ce_3TiX_5 and Ce_3VAs_5 systems.

	V (Å^3)	T_N (K)	Θ (K)	μ_{eff} (μ_B/Ce)	T_K (K)	γ (mJ/(Ce-mol·K^2))	ΔC (J/(Ce-mol·K))
Ce_3TiBi_5[31]	516	5	–114	2.58	5.3	210	5.2
Ce_3TiSb_5[30]	480	5.5	–198	2.47	8.3	199	4.7
Ce_3TiAs_5[32]	402	13	–55	2.76	11	215	1.2
Ce_3VAs_5	394	14	–160	5.29 (Tot.)	19	128	0.7

Note: The Kondo temperatures T_K for Ce_3TiSb_5 and Ce_3TiBi_5 are extracted from the heat capacity data in Refs. [30,31] and determined by the temperature where the magnetic entropy change reaches $0.5R\ln 2$ ignoring the entropy change below 2 K.

4. Conclusion

A new Ce-based compound Ce_3VAs_5 was synthesized under high-pressure and high-temperature conditions. It crystallizes in a hexagonal structure with the space group $P6_3/mcm$, featuring face-sharing VAs_6 octahedral chains and zig-zag Ce chains running along the c-axis. A magnetic transition is observed at $T_N = 14$ K, which is attributed to the Ce sublattice. Although V ions in Ce_3VAs_5 are suggested to carry local magnetic moments, no long-range magnetic ordering associated with the V sublattice has been detected down to 2 K. The Sommerfeld coefficient γ, derived from heat capacity measurements, is 128 mJ/(Ce-mol·K^2), indicating heavy-fermion behavior in this compound. An anomalous drop observed in the resistivity curve suggests the interplay between the crystal electric field (CEF) effect and Kondo scattering. Owing to its quasi-1D structural character, Ce_3VAs_5 is expected to exhibit an anisotropic Kondo effect, warranting further investigation in future studies.

Acknowledgements

This work was supported by the National Key Research and Development Program of China (Grant Nos. 2024YFA1408000 and 2023YFA1406001) and the National Natural Science Foundation of China (Grant No. 12474097).

References

[1] Steglich F, Aarts J, Bredl C D, Lieke W, Meschede D, Franz W and Schafer H 1979 *Phys. Rev. Lett.* **43** 1892
[2] Movshovich R, Graf T, Mandrus D, Thompson J D, Smith J L and Fisk Z 1996 *Phys. Rev. B* **53** 8241
[3] Shen B, Zhang Y, Komijani Y, Nicklas M, Borth R, Wang A, Chen Y, Nie Z, Li R, Lu X, Lee H, Smidman M, Steglich F, Coleman P and Yuan H Q 2020 *Nature* **579** 51
[4] Hegger H, Petrovic C, Moshopoulou E G, Hundley M F, Sarrao J L, Fisk Z and Thompson J D 2000 *Phys. Rev. Lett.* **84** 4986
[5] Stewart G R 1984 *Rev. Mod. Phys.* **56** 755
[6] Mathur N D, Grosche F M, Julian S R, Walker I R, Freye D M, Haselwimmer R K W and Lonzarich G G 1998 *Nature* **394** 39
[7] Wirth S and Steglich F 2016 *Nat. Rev. Mater.* **1** 16051
[8] Guo D L and Li H 2025 *Chin. Phys. B* **34** 067102
[9] Zhang J W, Wu J Y, Chen Y, Li R, Smidman M, Liu Y, Song Y and Yuan H Q 2024 *Chin. Phys. Lett.* **41** 127304
[10] Li F L, Yu T Y, Lai J W, Liu J X, Liu P T, Chen X Q and Sun Y 2024 *Chin. Phys. Lett.* **41** 107301
[11] Doniach S 1977 *Physica B & C* **91** 231
[12] Nakatsuji S, Pines D and Fisk Z 2004 *Phys. Rev. Lett.* **92** 016401
[13] Yang Y F, Fisk Z, Lee H O, Thompson J D and Pines D 2008 *Nature* **454** 611
[14] Yang Y F and Pines D 2008 *Phys. Rev. Lett.* **100** 096404
[15] Yang Y F 2016 *Rep. Prog. Phys.* **79** 074501
[16] Zhang J, Wang X C, Zhou L, Liu G X, Adroja D T, da Silva I, Demmel F, Khalyavin D, Sannigrahi J, Nair H S, Duan L, Zhao J F, Deng Z, Yu R Z, Shen X, Yu R C, Zhao H, Zhao J M, Long Y W, Hu Z W, Lin H J, Chan T S, Chen C T, Wu W and Jin C Q 2022 *Adv. Mater.* **34** 2106728
[17] Zhang J, Zhang X Y, Xia Y H, Zhao J F, Duan L, Wang G D, Min B S, Cao H B, Dela Cruz C R, Zhao K, Sun H Y, Zhu J L, Zhang J F, Xiang T, Wang X C and Jin C Q 2023 *Phys. Rev. B* **108** 174423
[18] Zhang J, Jia Y T, Chen X M, Min B, Honda T, Hu Z, Tjeng L H, Shamoto S I, Zhao J F, Deng Z, Song J, Duan L, Valvidares M, Zhu J L, Wang X C and Jin C Q 2025 *Phys. Rev. B* **111** 224405
[19] Zhang J, Komarek A C, Jin M, Wang X C, Jia Y T, Zhao J F, Li W M, Hu Z W, Peng W, Wang X, Tjeng L H, Deng Z, Yu R Z, Feng S M, Zhang S J, Liu M, Yang Y F, Lin H J, Chen C T, Li X D, Zhu J L and Jin C Q 2021 *Phys. Rev. Mater.* **5** 054606
[20] Duan L, Wang X C, Zhang J, Zhao J F, Cao L P, Li W M, Yu R Z, Deng Z and Jin C Q 2020 *Chin. Phys. B* **29** 036102
[21] Zhang J, Duan L, Wang Z, Wang X C, Zhao J F, Jin M L, Li W M, Zhang C L, Cao L P, Deng Z, Hu Z W, Agrestini S, Valvidares M, Lin H J, Chen C T, Zhu J L and Jin C Q 2020 *Inorg. Chem.* **59** 5377
[22] Zhang J, Jin M L, Li X, Wang X C, Zhao J F, Liu Y, Duan L, Li W M, Cao L P, Chen B J, Wang L J, Sun F, Wang Y G, Yang L X, Xiao Y M, Deng Z, Feng S M, Jin C Q and Zhu J L 2020 *Chin. Phys. Lett.* **37** 087106
[23] Duan L, Wang X C, Zhan F Y, Zhang J, Hu Z W, Zhao J F, Li W M, Cao L P, Deng Z, Yu R Z, Lin H J, Chen C T, Wang R and Jin C Q 2020 *Sci. China Mater.* **63** 1750
[24] Duan L, Wang X C, Zhang J, Zhao J F, Li W M, Cao L P, Zhao Z W, Xiao C J, Ren Y, Wang S, Zhu J L and Jin C Q 2021 *Chin. Phys. B* **30** 106101
[25] Duan L, Wang X C, Zhang J, Hu Z, Zhao J F, Feng Y G, Zhang H L, Lin H J, Chen C T, Wu W, Li Z, Wang R, Zhang J F, Xiang T and Jin C Q 2022 *Phys. Rev. B* **106** 184405
[26] Wang Z L, Wang G D, Li W M, Chen R T, Duan L, Zhao J F, Deng Z, Zhang J F, Yan T J, Zhang J, Wang X C and Jin C Q 2025 *Chin. Phys. B* **34** 086101
[27] Xu Z C, Wang Y X, Zhang C W, Liu H X, Han X, Wu L S, Zhang X M, Wu Q S and Shi Y G 2024 *Phys. Rev. B* **110** 165106
[28] Zhang C W, Wang Y X, Zheng J X, Du L, Li Y, Han X, Liu E K, Wu Q S and Shi Y G 2024 *Phys. Rev. Mater.* **8** 034402
[29] Zhang C, Pang J, Dong G, Zhang S, Wu Q, Shi Y and Wang Y 2025 *Phys. Rev. Mater.* **9** 054404
[30] Matin M, Kulkarni R, Thamizhavel A, Dhar S K, Provino A and Manfrinetti P 2017 *J. Phys.: Condens. Matter* **29** 145601
[31] Motoyama G, Sezaki M, Gouchi J, Miyoshi K, Nishigori S, Mutou T, Fujiwara K and Uwatoko Y 2018 *Physica B* **536** 142
[32] Fu L C, Shi L C, Chen X M, Duan L, Peng Y, Zhang J, Song J, Deng Z, Zhang S J, Zhao J F, Liu Y, Zhang J F, Zhu J L, Wang X C and Jin C Q 2025 *J. Phys.: Condens. Matter* **37** 015803
[33] Tsubouchi M, Motoyama G, Gouchi J, Miyoshi K, Nishigori S, Fujiwara K, Mutou T and Uwatoko Y 2020 *JPS Conf. Proc.* **30** 011102
[34] Ritter C, Pathak A K, Filippone R, Provino A, Dhar S K and Manfrinetti P 2021 *J. Phys.: Condens. Matter.* **33** 245801
[35] Motoyama G, Shinozaki M, Nishigori S, Yamaguchi A, Aso N, Mutou T, Manago M, Fujiwara K, Sumiyama A and Uwatoko Y 2023 *JPS Conf. Proc.* **38** 011084

52023 *JPS Conf. Proc*. 011084
[36] Gauthier N, Sibille R, Pomjakushin V, Fjellvag Ø S, Fraser J, Desmarais M, Bianchi A D and Quilliam J A 2024 *Phys. Rev. B* 109 L140405
[37] Toby B H and Von Dreele R B 2013 *J. Appl. Crystallogr.* **46** 544
[38] Moore S H D, Deakin L, Ferguson M J and Mar A 2002 *Chem. Mater.* **14** 4867
[39] Takeuchi T, Hashimoto S, Yasuda T, Shishido H, Ueda T, Yamada M, Obiraki Y, Shiimoto M, Kohara H, Yamamoto T, Sugiyama K, Kindo K, Matsuda T D, Haga Y, Aoki Y, Sato H, Settai R and Önuki Y 2004 *J. Phys.: Condens. Matter* 16 L333
[40] Wang L, Fu Z, Sun J, Liu M, Yi W, Yi C, Luo Y, Dai Y, Liu G, Matsushita Y, Yamaura K, Lu L, Cheng J G, Yang Y F, Shi Y and Luo J 2017 *Npj Quantum Mater.* **2** 36
[41] Hayashi Y, Takai S, Matsumura T, Tanida H, Sera M, Matsubayashi K, Uwatoko Y and Ochiai A 2016 *J. Phys. Soc. Jpn.* **85** 034704
[42] Fu L C, Cheng W J, Shi L C, Min B S, Peng Y, Zhang J, Song J, Deng Z, Zhao J F, Liu Y, Zhu J L, Zhang J F, Wang X C and JinC Q 2026 *Chin. Phys. Lett.* **43** 010705